

Protection Function Assessment of Present Relays For Wind Generator Applications

Jose J. Chavez, Marjan Popov, Alexander Novikov, Sadegh Azizi and Vladimir Terzija

Abstract— The settings and the protection functions of the relays are established by the TSOs based on networks with only synchronous generation or with power electronic devices with low level of penetration. In the recent years, the integration of renewable generators through partial or full-scale power electronics has been considerably increased. Renewable generators, depending on the demand are capable of fast switching so that their output current can be controlled during a load change in the grid. Although power electronic devices show good performance in terms of power support, the control strategy and its electrical architecture highly influence short-circuit current characteristic during faults. The waveforms of the fault currents with renewable generators differ significantly from those with conventional synchronous generators. During unbalanced faults, the reliability and the dependability of the relay may significantly decrease. In this paper, the performance of classical protection functions of two commercial relays (denoted as A and B) are investigated. The relays are tested in a Hardware-In-the-Loop environment and the strengths and weaknesses of these functions are determined. The results shown in this paper can be used as an overview of the actual protection device performances for different scenarios.

Index Terms—Directional protection, Distance protection, Line differential protection, Renewable generators.

I. INTRODUCTION

CONVENTIONAL protection functions have been very reliable during years and even today play a major role for fault detection and identification. Current microprocessor based relays are able to operate by combining two or more protection functions like differential, distance, overcurrent etc. For traditional grids composed of synchronous generators (SGs), actual protection devices perform with very high level of reliability [1]. Nevertheless, we cannot say that they will show the same level of performance in future power systems with high renewable generator (RWG) penetration.

It is well known that the existing grids are undergoing major changes with the inclusion of RWGs. In fact, according to REN21 [2] in 2017, 24.5% of the total power energy

produced around the world was renewable with 16.6% resulting from hydropower plants and 7.9% from converter-based distribution generators. The power electronics (PE)-based RWGs were used as disperse generation in distribution systems and recently, the energy produced by renewables has been significantly increased. It is expected that the penetration level of the distribution generation in the years to come will further increase.

The large scale of PE converters may sustain the stability of the power grid but may jeopardize the operation of the protective relays. Some problems with classical functions in actual grids were firstly reported in [3]. These are problems such as protective device coordination due to infeed and bi-directional current flow, synchronizing and autoreclosing as well as issues related to ground fault detection when distributed resources are connected to the grid. In [4], the wind power variation related to distance protection was studied. Voltage and current frequency discrepancy for a transmission line (TL) next to wind farm, which affects severely the performance of distance protection relays was analyzed in [5]. The effect of fault current frequency of a doubly fed induction generator (DFIG) that jeopardizes the operation of distance protection was reported in [6]. A distance relay failures near a Type-4 wind farm and possible solutions were discussed in [7] and [8] respectively. The performance of the distance protection in bulk wind generator systems was investigated in [9], [10] and ground fault protection issues were discussed in [11].

This paper reports the performance of actual protection relays applied in existing and forthcoming scenarios with high penetration of PE. In this context, the protection functions of differential, distance and directional protection for 2 different vendor relays are tested by applying real time Hardware-in-the-Loop (HiL) tests. The benchmark system is developed in an Electromagnetic transient based real-time simulator in a way to easily change the conditions of the grid. Nearly 5,000 simulation cases were performed following the recommendations provided in IEC 60255-121:2014 standard [12]. The results are well documented and classified.

II. POWER SYSTEM DESCRIPTION AND HiL TEST PLATFORM

Classical protection functions are tested in a HiL system as summarized in Fig. 1. The power system is developed in RTDS/RSCAD environment in a way to easily change its configuration and combine RWG and/or SG (see Fig. 2). Overall the simulation is performed with a 50 μ s time step.

“This project has received funding from the European Union’s Horizon 2020 research and innovation program under grant agreement No 691800”

J.J. Chavez, M. Popov, and A. Novikov are with Delft University of Technology, Delft, 2628CD the Netherland (e-mail: j.j.chavez@muro.tudelft.nl; M.Popov@tudelft.nl).

S. Azizi is with the School of Electronic & Electrical Engineering, University of Leeds, LS2 9JT, UK (e-mail: S.Azizi@leeds.ac.uk)

V. Terzija is with School of Electrical and Electronic Engineering, The University of Manchester, Manchester, M13 9PL, U.K. (e-mail: vladimir.terzija@manchester.ac.uk).

Paper submitted to the International Conference on Power Systems Transients (IPST2019) in Perpignan, France June 17-20, 2019.

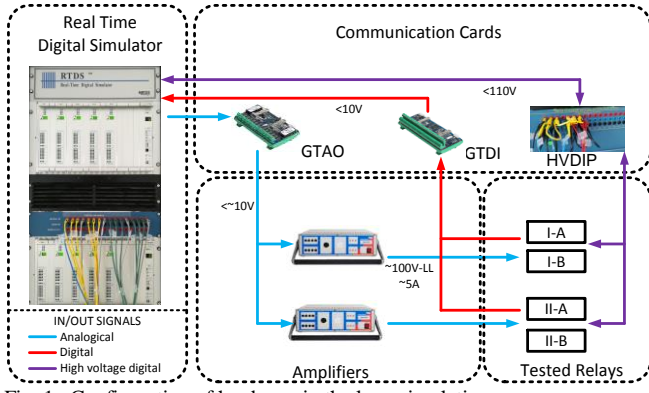


Fig. 1. Configuration of hardware in the loop simulation.

TABLE I
TEST CASES

Scenario	Differential	Directional	Distance	Type
Grid	2	2	2	Strong, Weak
Generator level	2	2	2	40MW, 200MW
Scenario	2	2	2	SG, RWG
Point of line	3	2	7	
Type of fault	4	4	4	LN, LLN, LL, and LLL
Impedance	3	3	3	0 Ω , 1 Ω , 10 Ω
Repetitions	3	3	3	
Total	864	576	2016	3456

However, for the wind turbine type-3 (RWG generator) a small time step of 1.4 μ s is used.

A. System Description

Among other features, the system is connected to a grid with the possibility of modifying its strength from a strong to a weak grid. Besides, the generator is connected to the outgoing transmission line in the grid, and there are another 2 generators that can be changed from a SG to a RWG in a straightforward manner. In this way, this feature is capable of adapting the scheme with different types of generations and with different penetration levels. The network can also be upgraded with synchronous generation, Photovoltaic (PV) generation and Type-4 wind generator as explained in [13]. However, in this paper the test network shown in figure 2 is used to study the protection performance of Type-3 generator. Its turbine control has been developed according to [14] where a main and auxiliary controllers are used. The main control at the grid side converter (GSC) is based on the requirements of a DC voltage regulation and reactive power support state by the grid code. For the rotor side converter (RSC), the requirements are the optimal torque and the reactive power support. The auxiliary control (activated when unbalance voltage is detected) is designed for negative sequence and is based on 2ω oscillation minimization at GSC and RSC.

The outgoing TL, Bergeron model, is 30.5 km long with positive and zero sequence impedances equal to $R_1 = 0.0293\Omega/\text{km}$, $XL_1=0.3087\Omega/\text{km}$, $XC_1=0.2664\text{M}\Omega/\text{km}$ and $R_0 = 0.3\Omega/\text{km}$, $XL_0=0.988\Omega/\text{km}$, $XC_0=0.4369\text{M}\Omega/\text{km}$. The

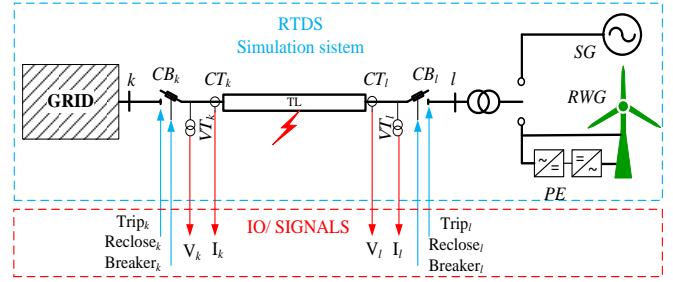


Fig. 2. Single line diagram test system, k and l outgoing ends TL.

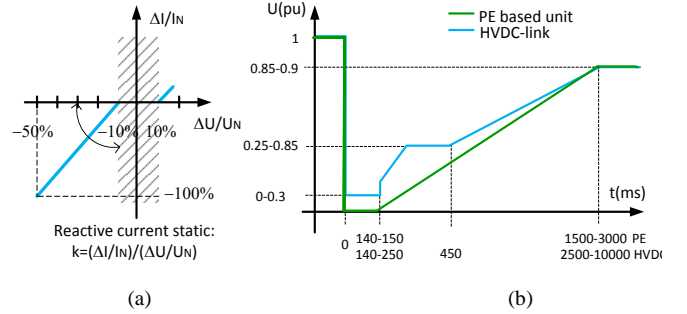


Fig. 3. Grid code a) Dynamic current requirements and b) Low voltage ride through.

SG or RWG is connected by a 225MVA, 33kV-400kV transformer. More details about the grid can be found in [13].

Due to the large power delivered by RWG, it is not allowed to be disconnected immediately from the grid during faults or temporary voltage drops [15]. For these reasons and in order to ensure system stability and security of supply, the TenneT grid code [16] in accordance to ENTSO-E [17] is taken into account. The grid code with respect to voltage support and reactive power injection is considered in this work, however, fault ride through capability is not considered as the goal is to investigate the performance of the relay with respect to Zone-1 and Zone-2 operation.

1) Voltage Support during and after Faults

According to [16], dynamic voltage support is mandatory during short-term voltage drop or rise. The relation between the voltage drop/rise and the current support is linear as it can be seen in Fig. 3(a). During voltage drops equal to 50% of the steady-state value, the RWGs inject at least 1.0 pu reactive current, whilst during overvoltage, reactive current withdraw is required. A dead-band of 10% is taken to avoid undesirable control actions. After the voltage level returns to the dead band, the voltage support must be maintained for 500ms in accordance with the specified RWG characteristic. The transient balancing procedures following the voltage return must be completed after 300ms.

2) Low Voltage Ride Through

Fig. 3(b) shows the RWG LVRT profile during a three-phase fault. Symmetrical voltage dips must not lead to instability or disconnection of the generation plant from the grid. In case of a fault that lasts for more than 150 ms, with a nearly zero voltage deep, the RWG should switch to a blocking condition and be disconnected from the system. The TL protection function follows the grid code and does not disconnect the RWG during an external short circuit fault.

Since we test the protection performance, the fault ride through option is disabled.

B. Hardware In the Loop System Description

As illustrated in Fig. 1, the HiL system consists of a real-time simulator (RTS), analog/digital communication cards, two CMS 156 Omicron® amplifiers, and four relays from two different manufacturers. There are three types of signals used to exchange data between the RTS and the relays. *Analog signals*: currents, and voltages are sent out from RTS via the analog output (GTAO) card. The signals voltages at this stage are lower than 10 V. These voltages are amplified, which make the secondary signals from ideal current transformers (CT) and ideal voltage transformers (VT) used at each end of the protected TL (k, l). Eight measured inputs are available on the relays side: three phase-to-earth voltages, one input for the displacement voltage from the VT, three phase currents and the earth current from the CT. *Binary signals*: trip and reclosing commands from the relays are collected by RTS via digital input (GTDI) card. *Binary high voltage signals* (~110 V) from the breaker status are interchanged from RTS to the relays by the high voltage front panel (GTFPI). Relays are tested for different scenarios according to TABLE I. The necessary changes in the system are automatized by making use of a runtime script file for batch mode simulations.

III. LINE DIFFERENTIAL PROTECTION FUNCTION BASIC PRINCIPLE & TEST PROCEDURE

The numerical relays with two or more functions are currently regularly used for protection of transmission lines. For 220 kV and higher, the differential protection is set as a primary function, the distance protection as a backup and the directional as a complement of the distance protection [12]. When a communication channel is not available, the distance function is used as the main protection.

The differential function is based on current comparison (current Kirchoff law). According to Fig. 2 and Fig. 4(a), relays are located in buses k and l . Relay k measures and exchanges the electrical signals via a communication channel to relay l . The measured quantities are compared in normal state; the current entering to the TL is close or equal to the current leaving it, and in this case, the differential current magnitude is nearly zero, and out of tripping zone as shown in Fig. 4(b). During a fault on the TL, the differential current is different than zero. To deal with measurement errors such as signal jitters, or response characteristic of CT/VT, the line differential protection algorithms employ restrained characteristics (I_{res} in Fig. 4(b)) avoiding tripping signals when differential current is different to zero in healthy operation. In the context of this section, Line Differential Protection Test Procedure is explained.

According to TABLE I, the line differential protection was tested 864 times. Two scenarios were tested, 100% SG and 100% RWG. Two types of grids (a strong and a weak) and three fault locations at 65%, 95% and outside the TL were simulated. Fig. 5 shows the relay results for a weak system case and bolted faults at 65% and 95% of TL. The continuous line represents the scenario when only SGs are used in the system and the dashed line corresponds to the high RWG

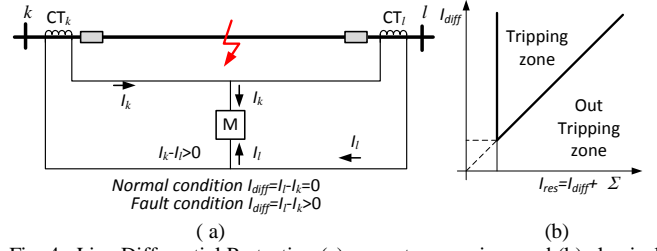


Fig. 4. Line Differential Protection (a) current comparison and (b) classical characteristic vs restrained current.

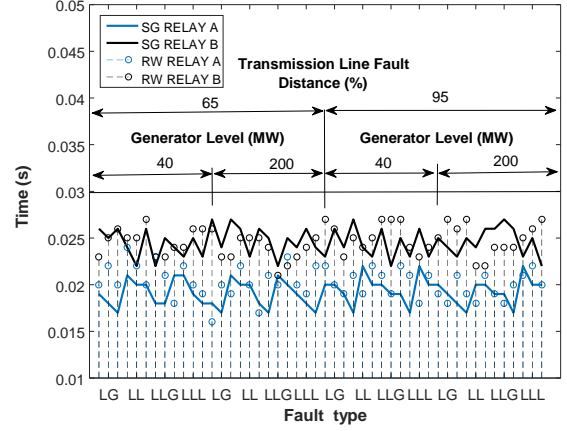


Fig. 5. Differential protection function, Relay performance in a system with high PE-based RWGs.

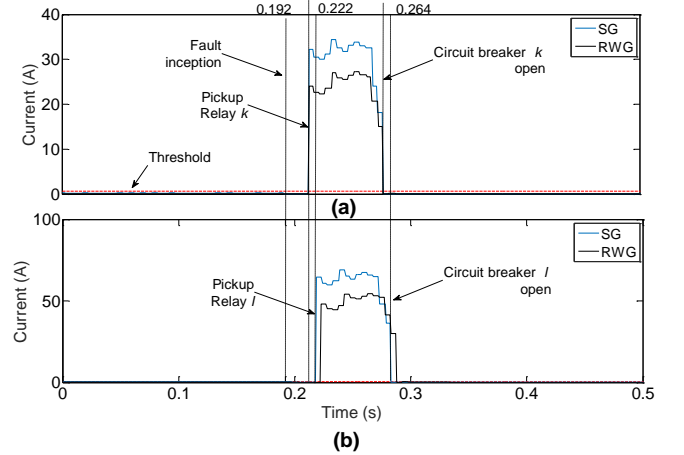


Fig. 6. Line Differential Protection current during a single-LG fault at 70% of the TL PE and SG scenarios. (a) Current i_{diffA} at bus k (grid) and (b) Current i_{diffA} at bus l .

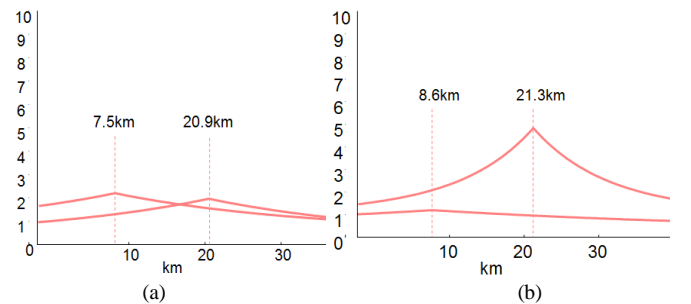


Fig. 7. Fault distance calculation by the Differential function taken from one relay during a LG fault 70% TL. (a) PE-based generator 40MW and (b) SG 40MW.

penetration scenario. For all the cases both relays operated instantaneously and no fault trip was missed.

In the RWG scenario, the average speed for the relays was 0.0202 s, and 0.0247 s for **A** and **B** relay respectively, and for a SG scenario the average speed was 0.0192 s and 0.0245 s for relays **A** and **B**. The faster trips in relay **A** are recorded during SG scenario (see continues blue line in Fig. 5). Additionally, the automatic reclosing function is set to be executed after 1 s. Fig. 6 shows the differential secondary current in phase A during SLG fault RWG case. It can be seen that the relays at k , the nearest to the grid, have a pick-up time ~ 20 ms after the fault inception and ~ 10 ms before the relays at l . In fact, k relay computes the fault faster and sent the trip command to relay l . Another relay's characteristic used in the differential protection is the ability to compute the fault distance. For all cases and for both relay types, the computed fault distances are near to the fault inception. Fig. 7 shows the computed fault distance during a LG bolted fault at 70% of the TL for (a) SG case and for (b) RWG case.

IV. DIRECTIONAL EARTH OVERCURRENT FUNCTION BASIC PRINCIPLE & TEST PROCEDURE

Directional earth overcurrent relays have been commonly used to detect the fault direction. The basic principle of torque magnitude used in mechanical relays has been mimicked in numerical relays [18] to establish forward and reverse operating regions as it can be seen in Fig. 8(a). They use the phase relationship of voltage and current to determine the fault direction. The zero sequence current ($3I_0$) that can be measured or computed is used as a reference variable. As $3I_0$ current results from fault current components in all phases, in order to obtain directional performance, this current must be compared to other related current magnitudes known as polarizing quantities.

The zero sequence voltage ($3V_0$) is widely used as a polarizing quantity, although other magnitudes such as the negative voltage ($3V_2$), or negative current ($3I_2$) can be used when the system cannot supply enough zero sequence voltage. The test procedure of Directional Earth Overcurrent Protection is explained below.

In case of earth fault protection, only the relays at one end of the transmission line are needed; at the nearest RWG bus (l). According to TABLE I, this function is tested 576 times and the faults are simulated at two locations; 65% of the TL (forward) and behind the relay (0% backward) to test the protection in forward and reverse zones with impedance set to 150 Ω . This function is used as a local backup and with a threshold current equal to 0.4 A and 600 ms trip time. The fault detection of relays **A** and **B** are with accuracy of 97% and 98% respectively.

In this work, two cases are reported, namely a 100% SG and RWG case during a LLG fault at 65% of the TL. The sequence signals from relay **A** are shown in Fig. 8 (b), and it can be seen the forward fault. The sequence currents can be seen in Fig. 9. Besides, the differences in the amplitude of I_0 and the wave shapes are similar. Major differences can be seen in I_1 and I_2

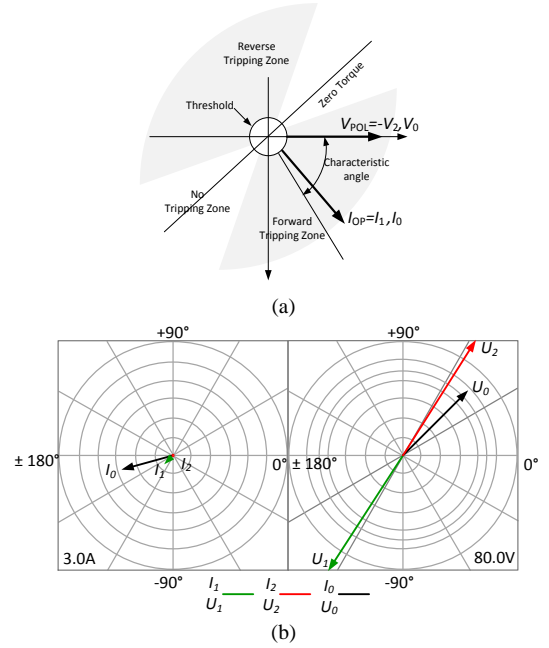


Fig. 8. Directional characteristic (a) Forward and reverse zones and (b) Circular diagram of sequence currents and voltages from relay **A** during RWG scenario for LLG fault.

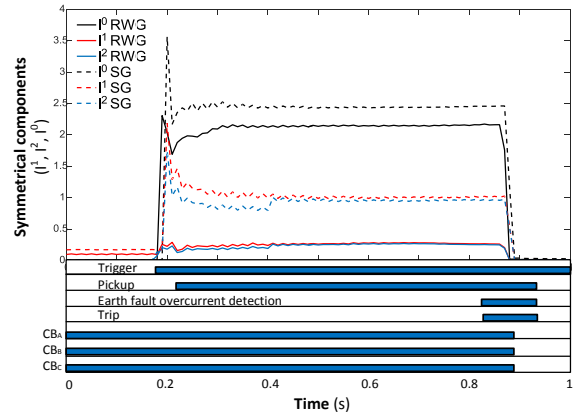


Fig. 9. Directional Earth Overcurrent function sequence currents and relay binary signals for SG and RWG cases during a LLG fault

sequences where current magnitudes are almost suppressed in case when RWG is in operation. The average time for tripping action is equal to 605 ms and 608 ms for relays **A** and **B** respectively. In Fig. 9, the currents and the binary signals from the relay are plotted and CB corresponds to status breaker.

V. DISTANCE PROTECTION FUNCTION BASIC PRINCIPLE & TEST PROCEDURE

The distance protection relay function makes use of complex algorithms. These algorithms are used to detect fault conditions, to identify the faulted phase and to compute the fault impedance. Basically, protection function measures the positive sequence impedance (R and X or Z and θ) from the protection measuring point to the fault [19]. As the impedance is proportional to the TL length, it is possible to compute the distance of the fault from the impedance seen by the relay [19].

Some manufacturers employ superimposed quantities to detect the faulted phases [19], and others establish relations

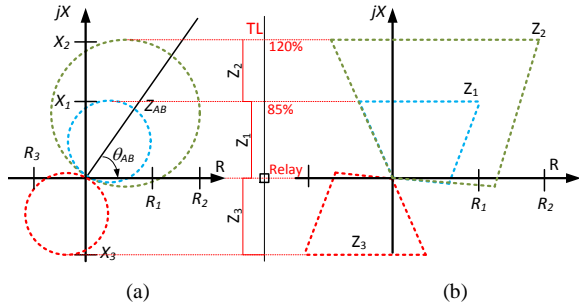


Fig. 10. Distance relay operation zones shapes (a) Mho or admittance and (b) quadrilateral characteristics.

between the angles of negative sequence and the zero sequence currents in order to determine which of the impedance loops must be activated [19]. The way each manufacturer determines the fault may differ significantly.

A. Mho Characteristic

In Fig. 10(a), the self-polarized Mho element for the system is represented as a circle on the impedance plane. The diameter of this circle extends from the origin of the plane to the relay reach setting zone (Z_n) on bolted fault locus [20]. If no arc impedance is assumed, the computed impedance for a fault in the vicinity of the relay is near to zero. If the measured impedance is plotted for a LLL fault at each point along the TL, it will produce a bolted fault locus with the same angle as the TL impedance [21].

B. Quadrilateral Characteristic

High impedance faults are more likely to occur during single phase faults. Since in this case the resistive operation area increases, the quadrilateral characteristic, shown in Fig. 10(b) is more suitable to be used.

C. Protected Zones

As shown in Fig. 10, two zones are covered: Zone 1, reaches up to 80% of the line impedance taking into account the CT and VT errors. The recommended time delay is 0 s to 40 ms. Zone 2 is used as a local backup protection. The typical setting of Zone 2 is up to 120% of the line impedance with a time delay equal to 400 ms..

D. Distance Protection Test Procedure

According to Table I, relays **A** and **B** at bus *l* with the distance protection as a primary function are tested 2016 times with different topologies of the system and bolted faults at 0%, 50%, 75%, 85%, 90%, and 100% distance of the TL. Fig. 11 shows the comparison of the relays from two different vendors summarizing the percentage of missed and delayed trips. Comparing to the previous protection functions for the same test case, the relays experienced difficulties when RWG is in the covering bus. During LL faults in approximately 50% of the cases, the relays do not trip and in approximately 20% they experience delayed trips. The tests also reveal that there are also failures to trip and delayed trips during LLL and LLG faults. The relays compute in most cases the impedance trajectory successfully when the relay failed to trip. The tests reveal that starting was the problem and by decreasing the

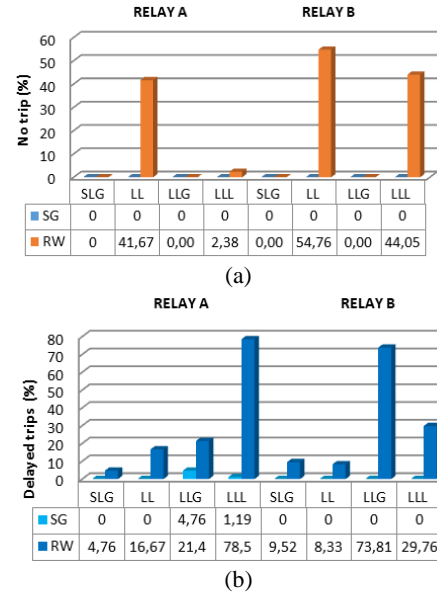


Fig. 11. Distance protection function behavior (a) No trip and (b) delayed trips.

starting current, only one relay tripped with delay. Anyhow, for low infeed power even low starting current could not trip the relay.

Fig. 12 shows three interesting cases with a power flow location from the RWG toward the network. Fig. 12 (a) shows a *trip command case*; the impedance trajectory slowly enters protection zone Z_1 , the square markers denote the measured impedance sampling. There are at least three measurements before the trajectory reaches Z_1 . This case corresponds to an outgoing 40MW SG and the relay performs correct with respect to zone and trip command. Fig. 12 (b) shows a *delayed trip case*; in this case the impedance trajectory constantly enters and leaves the protection zone until the trip action is executed. It corresponds to an outgoing 200 MW Type-3 wind generator. The converter used to control the RWG changes the short-circuit current and thus the impedance trajectory. The fault is located at 70% of the TL and the trip action is not executed instantaneously but with a delay. Fig. 12 (c) shows a *fail to trip case*; this case corresponds to an outgoing 40 MW Type-3 wind generator. In this case, the impedance trajectory suddenly drops in Z_1 without previous measurement points. In fact, the fault trajectory changes from steady state to Z_1 in less than 3 measurement points (~ 3 ms). The trip action is generated after all the conditions are fulfilled. These conditions are fault detection, faulted phase identification, directionality, and impedance is inside the tripping range.

VI. CONCLUSIONS

A. Line differential function

Line differential protection works correctly for all the scenarios tested. Both relays are highly reliable and fault distance is well determined. Nevertheless, relay **A** that is near to the grid always picks up faster and sends the trip command to the other relay **A**. The sensitivity is not a constraint in this function.

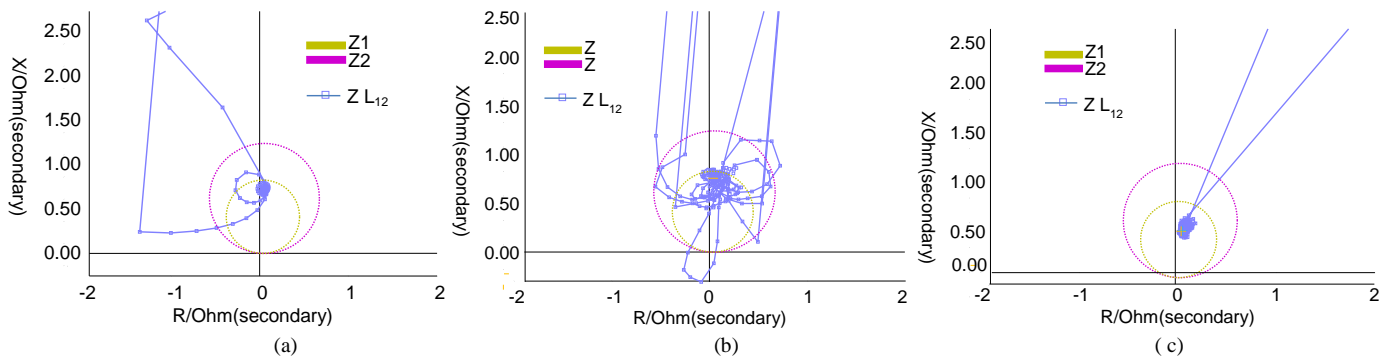


Fig. 12. Mho characteristic and impedance trajectory. Line to Line fault at 70% of the transmission line, 0Ω scenarios: (a) 40MW SG at bus l (b) 200MW RWG at bus l , and (c) 40 MW RWG at bus l .

B. Ground directional overcurrent function


Correct behavior of this protection have been observed with fault resistances of 150Ω , 75Ω and 0Ω . The positive sequence voltage polarization holds the memory long enough time and operates successfully even during close LLL faults.

C. Distance function

A higher number of unexpected results, in terms of missed and delayed trips are recorded. Due to the different distance protection algorithms implemented by the vendors, the distribution of unexpected results is not the same for both relays. Some of them experience more difficulties with LLL than LL faults. Despite this, LL faults have been found as the most problematic faults to be detected by the investigated distance relays. LLG faults due to the grounding of the transformers, are detected, however, a high number of delayed trips are also registered. The fault current level during the fault can help detecting it, but short-circuit current is not the only indicator that should be fulfilled by the protection function as directionality declaration, phase selection and impedance threshold are important for selective fault detection.

During the fault period, the impedance trajectory results in a delayed trip signal for some milliseconds (see Fig 12 (b)). It is found that even though the starting current is decreased to a very low level, the relays fail to detect the fault. Performed results reveal that there are still open questions and more work should be done to develop refined fault detection algorithms.

ACKNOWLEDGMENT

 This research was carried out as part of the MIGRATE project. This project has received funding from the European Union's Horizon 2020 research and innovation program under grant agreement No 691800.

REFERENCES

- [1] Standard for Interconnecting Distributed Resources with Electric Power Systems, IEEE, July 2003 (R2008).
- [2] A. Zervos, et. al. "Renewables 2017 global status report," REN21 Secretariat, Paris France 2017.
- [3] T. Seegers, K. Birt, R. Beazer, M. Begovic, and K. Behrendt et al., "Impact of distributed resources on distribution relay protection," in *IEEE Power System Relaying Committee*, Aug. 2004 [Online]. Available: www.pes-psrc.org
- [4] A. K. Pradhan and Geza Joos, "Adaptive distance relay setting for lines connecting wind farms", *IEEE Tran. on Energy Conversion*, vol.22, no.1, pp.206-213, 2007.

- [5] Zhang Baohui, Zhang Jinhua, and Yuan Bo, "Impact of wind farm integration on relay protection (6): analysis of distance protection for wind farm outgoing transmission line," *Electric Power Automation Equipment*, vol.33, no.6, pp.1-6, 2013.
- [6] A. Hooshyar, M. A. Azzouz, and E. F. El-Saadany, "Distance protection of lines connected to induction generator-based windfarms during balance faults," *IEEE Trans. Sustain. Energy*, vol. 5, no. 4, pp. 1193-1203, Oct. 2014
- [7] A. Hooshyar, M. A. Azzouz, and E. F. El-Saadany, "Distance protection of lines emanating from full-scale converter-interfaced renewable energy power plants-Part I: problem statement," *IEEE Trans. Power Delivery*, vol. 30, no. 4, pp. 1770-1780, August 2015
- [8] A. Hooshyar, M. A. Azzouz, and E. F. El-Saadany, "Distance protection of lines emanating from full-scale converter-interfaced renewable energy power plants-Part II: solution," *IEEE Trans. Power Delivery*, vol. 30, no. 4, pp. 1781-1791, August 2015.
- [9] V. Telukunta, J. Pradhan, A. Agrawal et. al. "Protection challenges under bulk penetration of renewable energy resources in power systems: Review," *CSEE Power and Energy Systems*, vol. 3, no. 4, December 2017.
- [10] K. El-Arroudi and G. Joos, "Performance of interconnection protection based on distance relay for wind power distributed generation," *IEEE Trans. Power Delivery*, vol. 33, no. 2 pp. 620-629, April 2018.
- [11] M. Nagpal and C. Henville, "Impact of power-electronic sources on transmission line ground fault protection," *IEEE Trans. Power Delivery*, vol. 33, no. 1, pp. 62-70, February 2018.
- [12] IEC Measuring relays and protection equipment -Part 121: Functional requirements for distance protection 60255-121:2014
- [13] J. Chavez, M. Popov et. al, "Exposing available distance relay operations near high wind penetration," 9th Protection, Automation and Control (PAC) World Conference, Sofia, Bulgaria 2018.
- [14] L. Xu, "Coordinated Control of DFIG's Rotor and Grid Side Converters During Network Unbalanced," *IEEE Trans. Power Electronics*, vol. 23, no. 3, pp.1041-1049, May 2008.
- [15] M. Tsili and S. Papathanassiou, "A review of grid code technical requirements for windfarms", *IET Renewable Power Generation*, vol. 3, no. 3, pp.308-332, 2009.
- [16] Tnet TSO GmbH, Grid code -High and extra high voltage-, Status first November 2015.
- [17] ENTSO-E: Implementation Guideline For Network Code - "Requirements for Grid Connection Applicable to all Generators", 2013 online available: <http://www.entsoe.eu>.
- [18] J. Roberts, and A. Guzman "Directional Element desing and evaluation," in *21st annual Western protective relay conference*, Washington, Revised edition 2006.
- [19] E.O. Schweitzer and J. Roberts, "Distance relay design," *SEL J. Rel. Power*, vol. 1, no. 1, Jul. 2010
- [20] I. E. O. Schweitzer, "New Developments in Distance Relay Polarization and Fault Type Selection," in *16th Annual Western Protective Relay Conference*, Washington, 1989
- [21] D. D. Fentie, "Understanding the dynamic mho distance characteristic," in *69th Annual Conference for Protective Relay Engineers (CPRE)*, Texas, 2016